

Nonlinear Excitations, Stability Inversions and Dissipative Dynamics in Quasi-one-dimensional Polariton Condensates

J. Cuevas,¹ A.S. Rodrigues,² R. Carretero-González,³ P.G. Kevrekidis,⁴ and D.J. Frantzeskakis⁵

¹*Grupo de Física No Lineal. Departamento de Física Aplicada I. Escuela Politécnica Superior, Universidad de Sevilla, C/ Virgen de África, 7, 41011-Sevilla, Spain*

²*Departamento de Física/CFP, Faculdade de Ciências,*

Universidade do Porto, R. Campo Alegre, 687 - 4169-007 Porto, Portugal

³*Nonlinear Dynamical Systems Group,*Department of Mathematics and Statistics, and Computational Science Research Center, San Diego State University, San Diego CA, 92182-7720, USA*

⁴*Department of Mathematics and Statistics, University of Massachusetts, Amherst MA 01003-4515, USA*

⁵*Department of Physics, University of Athens, Panepistimiopolis, Zografos, Athens 157 84, Greece*

(Dated: June 5, 2018)

We consider the existence, stability and dynamics of the ground state and nonlinear excitations, in the form of dark solitons, for a quasi-one-dimensional polariton condensate in the presence of pumping and nonlinear damping. We find a series of remarkable features that can be directly contrasted to the case of the typically energy-conserving ultracold alkali-atom Bose-Einstein condensates. For some sizeable parameter ranges, the nodeless (“ground”) state becomes *unstable* towards the formation of *stable* nonlinear single or *multi* dark-soliton excitations. It is also observed that for suitable parametric choices, the instability of single dark solitons can nucleate multi-dark-soliton states. Also, for other parametric regions, *stable asymmetric* sawtooth-like solutions exist. Finally, we consider the dragging of a defect through the condensate and the interference of two initially separated condensates, both of which are capable of nucleating dark multi-soliton dynamical states.

I. INTRODUCTION

An important recent development that has spurred a new direction for the physics of Bose-Einstein condensation has been the observation of condensation phenomena for polaritons in semiconductor microcavities [1] at much higher temperatures than ultracold atomic Bose-Einstein condensates (BECs) [2, 3]. In the setting of exciton-polariton BECs, the condensing “entities” are excitons, i.e., bound electron-hole particles. When confined, these develop strong coupling with light, forming exciton-photon mixed quasi-particles known as polaritons [4]. The finite temperature formation of polariton condensates leads the quasi-particles to also possess a finite lifetime: in fact, they can only exist for a few picoseconds in the cavity before they decay into photons. Hence, thermal equilibrium can never be achieved and the system produces a genuinely far-from-equilibrium condensate, in which external pumping from a reservoir of excitons counter balances the loss of polaritons due to the above decay mechanism. Nevertheless, numerous key features of the superfluid character of the exciton-polariton condensates have been established, including the flow without scattering (analog of the flow without friction) [5], the existence of vortices [6] (see also Ref. [7] for vortex dipole dynamics), the collective dynamics [8], as well as remarkable applications such as spin switches [9] and light emitting diodes [10] operating even near room temperatures.

The pumping and damping mechanisms associated

with polaritons enable the formulation of different types of models. One of these, proposed in Refs. [11, 12] suggests the use of a single partial differential equation (PDE) for the polariton condensate incorporating the above mentioned loss-gain mechanisms. This model features a localized (within a pumping region) gain and a nonlinear saturating loss of polaritons; these are the fundamental differences of this setting from the standard PDE mean-field model, namely the Gross-Pitaevskii equation (GPE) used in the physics of atomic BECs [2, 3, 13]. In another class of models, which has been proposed in Refs. [14–16], the polaritons are coupled to the evolution of the exciton population; such models also display nonlinear diffusive spatial dynamics for the excitons.

In this work, our aim is to consider the quasi-one-dimensional (1D) dynamics of polariton BECs and to illustrate their *fundamental differences* from the more standard alkali-atom condensates. At this point we should mention that polariton condensates considered so far (also experimentally) have been intrinsically two-dimensional (2D) [17]. Nevertheless, using tight confinement along one, transversal, direction (i.e., highly anisotropic variants of the traditional parabolic traps) we envision rendering the polariton condensate effectively 1D [18]. In addition, a broader perspective for our considerations is that understanding the nonlinear dynamics and pertinent phenomenology in the 1D setting, may pave the way towards subsequently generalizing relevant considerations to the more realistic 2D case. The key phenomena that are reported herein are: a wide parametric interval of destabilization of the fundamental nodeless state of polariton BECs; a partial stability within this interval of excited states, in the form of dark solitons; the

*URL: <http://nlds.sdsu.edu>

spontaneous production of higher excited (multi-soliton) states from lower ones or even from nodeless states; the production of dark soliton trains by dragging of a defect through the polariton BEC (cf. the recent relevant 2D experimental results in Ref. [19]); and finally the formation of long-lived dark multi-soliton dynamical states through the interference of two separated polaritonic condensates in analogy with the atomic BEC case of Ref. [20].

The paper is organized as follows. In Section II we describe our model and setup, providing also a brief description of our methods. Section III is devoted to our detailed numerical investigations, and Section IV concludes our work, including some suggestions for possible future studies.

II. MODEL SETUP

In our analysis below, we consider the modified complex Gross-Pitaevskii model developed in Refs. [11, 12] suitably reduced to one spatial dimension:

$$i\partial_t\psi = \left\{ -\partial_x^2 + x^2 + |\psi|^2 + i[(\chi(x) - \sigma|\psi|^2)] \right\} \psi, \quad (1)$$

where ψ denotes the polariton wavefunction trapped inside a 1D harmonic potential, x^2 (the transverse direction, perpendicular to x , corresponds to the tight trapping axis mentioned above). The differences of Eq. (1) from the standard GPE appearing in the physics of atomic BECs can be traced to the presence of (i) the spatially dependent gain term with

$$\chi(x) = \alpha\Theta(x_m - |x|), \quad (2)$$

where Θ is the step function generating a symmetric spot of “radius” x_m and strength α for the gain and (ii) the nonlinear saturation loss term of strength σ . Estimates of the relevant physical time and space scales, as well as physically relevant parameter values, are given in Ref. [11]. We should also note in passing that although our results below are given in the context of Eq. (1), we have ensured that similar phenomenology arises in the model of Refs. [14–16], for suitable parametric choices. In other words, the phenomenology that is reported in this work is *generically* relevant to (1D) polariton BECs independently of model specifics.

In what follows, we will consider the stationary solutions of the quasi-1D model at hand, in the form $\psi(x, t) = \psi_0(x) \exp(-i\mu t)$ where μ is the dimensionless chemical potential, and the stationary state $\psi_0(x)$ is governed by the following ordinary differential equation:

$$\mu\psi_0 = \left\{ -\frac{d^2}{dx^2} + x^2 + |\psi_0|^2 + i[(\chi(x) - \sigma|\psi_0|^2)] \right\} \psi_0. \quad (3)$$

Importantly, the additional condition

$$\int dx (\chi(x) - \sigma|\psi|^2)|\psi_0|^2 = 0 \quad (4)$$

needs to be enforced as a population balance constraint. This self-consistently selects the particular value of the chemical potential once the other parameters (i.e., α , σ , x_m) are fixed. This is why some of our graphs of the solution branches below will feature μ as a function of other solution parameters, such as x_m . We note in passing the significant difference of this trait from the Hamiltonian atomic BEC case, where there exist monoparametric families of solutions as a function of μ . Once stationary solutions of the differential-algebraic system of Eqs. (3)-(4) are identified, their linear stability is considered by means of a Bogolyubov-de Gennes analysis. Namely, small perturbations [of order $O(\delta)$, with $0 < \delta \ll 1$] are introduced in the form

$$\psi(x, t) = e^{-i\mu t} \left[\psi_0(x) + \delta(a(x)e^{i\omega t} + b^*(x)e^{-i\omega^* t} \right],$$

and the ensuing linearized equation are then solved to $O(\delta)$, leading to the following eigenvalue problem:

$$\omega \begin{pmatrix} a(x) \\ b(x) \end{pmatrix} = \begin{pmatrix} L_1 & L_2 \\ -L_2^* & -L_1^* \end{pmatrix} \begin{pmatrix} a(x) \\ b(x) \end{pmatrix}, \quad (5)$$

for the eigenvalue ω and associated eigenvector $(a(x), b(x))^T$, where L_1 and L_2 are the following operators:

$$L_1 = -\mu - \frac{d^2}{dx^2} + x^2 + 2(1 - i\sigma)|\psi_0|^2 + i\chi(x),$$

$$L_2 = (1 - i\sigma)\psi_0^2.$$

Once the stationary solutions are found to be linearly unstable (i.e., $\text{Im}\{\omega\} \neq 0$), then the dynamical manifestation of the corresponding instabilities is monitored through direct numerical simulations of Eq. (1). In addition, in what follows, we have considered dynamical scenarios under which nonlinear excitations, such as single- or multiple-dark-solitons [13] can arise in the context of polariton BECs. Such excited states have been extensively studied in the context of atomic BECs [21], while they have been amply considered in recent experimental investigations in this context [20, 22, 23]. Additionally, motivated by relevant studies in atomic BECs [24, 25] and recent experiments in polariton condensates [5, 19, 26], we consider the nucleation of dark solitons by a moving defect, modeled by a (localized) potential; the latter, is assumed to be produced by a narrow laser beam of Gaussian shape, namely:

$$V_{\text{def}} = V_0 \exp(-(x - vt)^2/\epsilon^2), \quad (6)$$

where V_0 , v and ϵ represent the amplitude, speed, and width of the potential, respectively. We consider the fixed point solution of the modified GPE (1) in the presence of this second defect potential (in addition to the harmonic trap x^2) at the center of the trap. Then we evolve the system in time starting from this solution, dragging the defect through the system. This is similar in spirit to the recent experiments of Ref. [5, 19] (and to the recent theoretical investigation of Ref. [27]). Finally, we study an

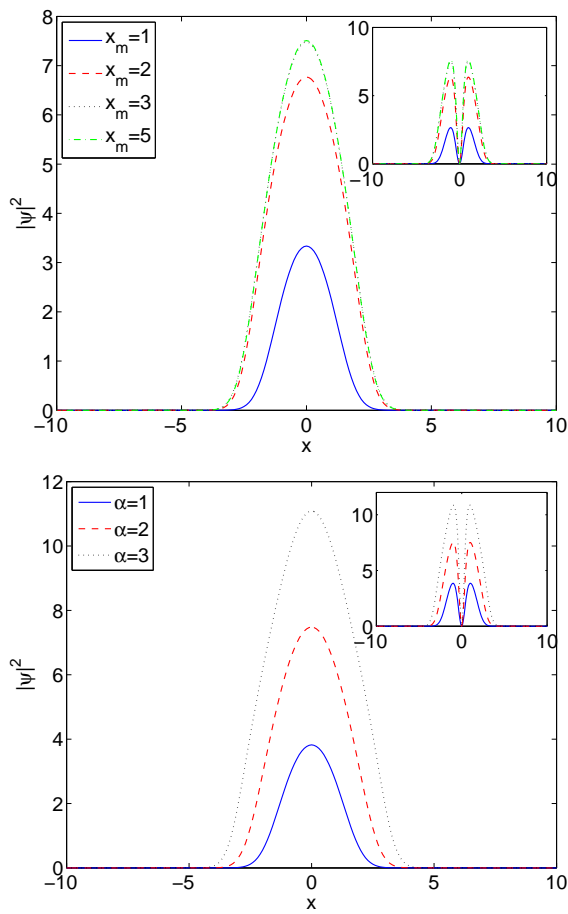


FIG. 1: (Color online) Spatial profiles of the densities, $|\psi|^2$, of nodeless states and single dark solitons (insets). In the top (bottom) panel, the parameter α (x_m) is kept fixed, taking the value $\alpha = 2$ ($x_m = 3$), while $\sigma = 3.5$ in both cases. As seen in the top panel, the profiles do not change appreciably above a critical value of $x_m \approx 3$: in fact, the profiles corresponding to $x_m = 3$ [dotted (black) line] and $x_m = 5$ [dotted-dashed (green) line] are almost indistinguishable from each other. All quantities in this and in all subsequent figures are dimensionless.

alternative proposal for dark soliton nucleation, akin to the interference experiments conducted for atomic BECs in Ref. [20], whereby a central potential barrier separating two polariton clouds is lifted allowing the two clouds to interfere; this process leads to the production of persistent dark solitons as well.

III. NUMERICAL RESULTS

We hereby explore the existence, stability and dynamical properties of the nodeless cloud (NC) as well as of excited states exhibiting a single-node, namely dark solitons (DSs). The above mentioned states (NC and DS) are the most fundamental nonlinear states of the system,

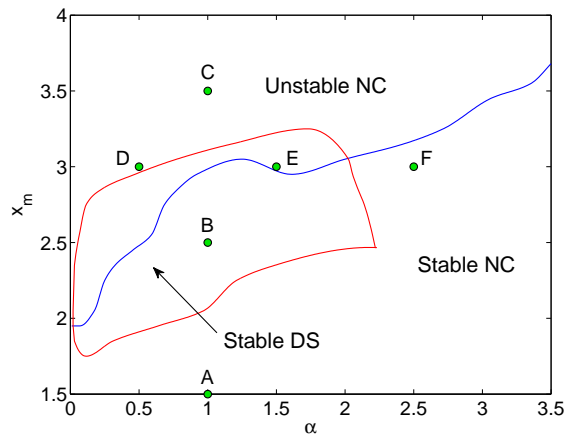


FIG. 2: (Color online) Stability domains of nodeless clouds (NC) and dark solitons (DS) for $\sigma = 0.35$ and $\alpha \leq 3.5$. Dark solitons are stable only in the area indicated by the arrow. Notice that there is a superposition between part of the dark soliton and nodeless cloud stability ranges. The (green) circles indicate the parameter locations for the spectra depicted in Fig. 3.

whose profiles—for different parameter combinations—are displayed in Fig. 1. In particular, the top panel of Fig. 1 depicts the NC and DS profiles for a constant saturation coefficient $\sigma = 3.5$ and constant pumping spot strength $\alpha = 2$, and a varying radius of the pumping spot x_m . We observe that, for given values of α and σ , there is a critical value of x_m above which the shapes of the NCs and DSs remain unchanged. In the example depicted in the top panel of Fig. 1, the profiles for $x_m \gtrsim 3$ are indistinguishable from each other (see profiles for $x_m = 3$ and $x_m = 5$). This effect is due to the fact that for large x_m , the pumping spot covers a larger portion than the saturated size of the cloud when loss and gain are balanced. This cloud size is the analogue of the Thomas-Fermi radius for an atomic condensate. The saturation of the cloud size is equivalent to the saturation of the chemical potential μ as x_m is increased, as shown below (see Figs. 4 and 5). In the bottom panel of Fig. 1 we depict the NC and DS profiles for a constant pumping spot radius $x_m = 3$ and a varying pumping spot strength. Note that, in this case, the size of the cloud continuously expands (in amplitude and width) with increasing spot strength.

We now proceed to provide a characterization of the existence and stability properties of the NC and DS profiles with respect to the various parameters at hand. In what follows, in order to offer a picture of the relevant parameter space, we have varied the gain parameters α and x_m whereas the coefficient of the saturating nonlinear loss $\sigma = 0.35$ has been kept fixed. Figure 2 depicts the existence and stability domains in the (α, x_m) parameter plane with $\sigma = 0.35$ fixed for both the nodeless cloud and the single DS that can be found as (numerically

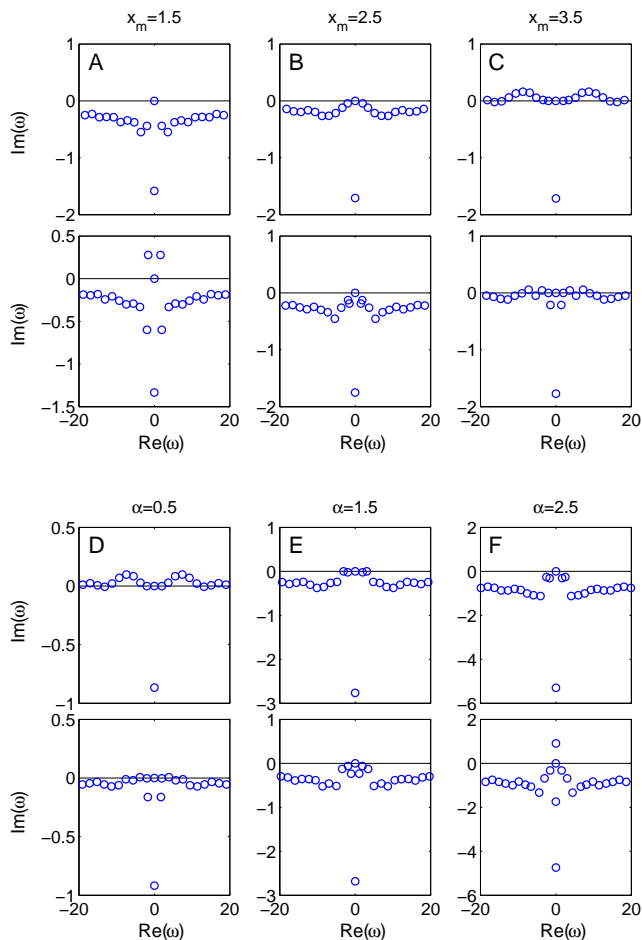


FIG. 3: (Color online) Spectral plane for nodeless clouds (top row in each series of panels) and dark solitons (bottom row in each series of panels) with $\sigma = 0.35$. The top series of panels correspond to fixed $\alpha = 1$ and increasing values of x_m as labeled whereas the bottom series of panels correspond to fixed $x_m = 3$ and increasing values of α as indicated. The different cases correspond to the parameter locations depicted by the (green) circles in Fig. 2.

exact up to a prescribed accuracy) fixed point solutions of Eq. (3). The NC and DS configurations exist for all parameter combinations, as it is the case for atomic condensates.

Nevertheless, as far as the stability and dynamical properties of NC and DS states are concerned, we can observe *fundamental* differences between the pumped-damped polariton BECs and atomic BECs. In particular, the nodeless cloud (which was *always* stable in the Hamiltonian case of atomic BECs [13]) *is now stable only below a critical value of the pumping spot size x_m* . On the other hand, also remarkably, even the single DS is stable only in a limited range, while it was *always* stable in quasi-1d harmonically trapped atomic BECs (see, e.g., Ref. [20] and references therein). Moreover, in a very unusual manifestation of stability inversions, not only can

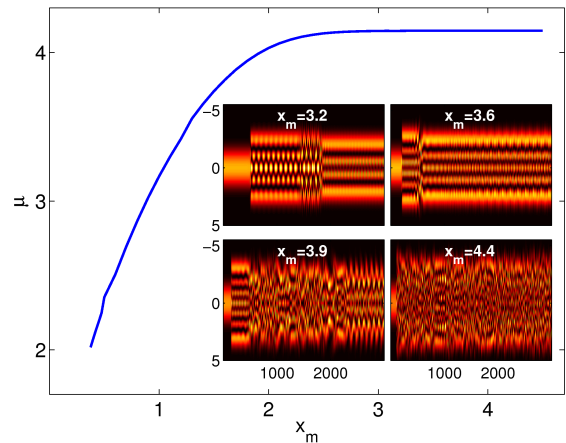


FIG. 4: (Color online) Top panel: Chemical potential as a function of x_m for a nodeless cloud with $\alpha = 1.0$ and $\sigma = 0.35$. The insets show the time evolution of the cloud for various values of x_m .

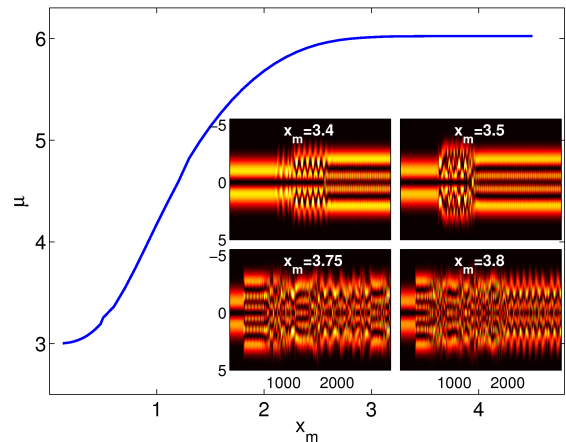


FIG. 5: (Color online) Top panel: Chemical potential as a function of x_m for a dark soliton with $\alpha = 1.0$ and $\sigma = 0.35$. The insets show the time evolution of the cloud for various values of x_m .

the nodeless state be stable while the dark soliton is not, but also vice versa: the state with a node can be stable while the one without a node is not. In Fig. 3 we show the details of the Bogolyubov spectra of both states. These showcase the dissipative nature of the dynamics being associated with frequencies chiefly with negative imaginary part; moreover, they also illustrate the potential instabilities arising in the system through Hopf bifurcations and oscillatory instabilities associated with complex eigenfrequencies, or through zero crossings (and purely imaginary eigenfrequencies). This second scenario only appears for dark solitons. From an intuitive viewpoint, this phenomenology can partially be understood on the following grounds. The condensate in the absence of the external driving has an intrinsic length scale selected by the trap

(and the chemical potential). The presence of the external forcing over the radius x_m introduces an additional length scale competing with the former one. Hence, when this forcing becomes fairly (spatially) extended, it favors a spatially wider state. This is manifested through the instability of a group of “background” spectral modes (which are not the lowest modes of the condensate close to the spectral plane origin) in the panels of Fig. 3. On the contrary, the dark soliton or multi-soliton states may become unstable through the same mechanism, or they may also become unstable through their “internal modes” [20] which lead to the isolated instability through the zero crossing.

In Fig. 4 we show a continuation of the nodeless state, for a fixed value of $\alpha = 1.0$. In particular, we depict the chemical potential μ as a function of pumping spot size, x_m . The insets show the dynamical evolution of the fixed point solution for several illustrative values of x_m , which reflect the different possible dynamical phenomena. The values shown are in the unstable domain of the NC. There are two types of behavior. The first behavior, for $3.1 < x_m < 3.8$, corresponds to the NC decaying into multiple-dark-solitons, by means of oscillatory transients (even in the region of stability of the single DS). The spontaneous emergence of these states from a nodeless one is a feature particular to polariton BECs, having no analog in the atomic BEC case. On the other hand, a second behavior, corresponds to values $x_m > 3.8$: in this case, even though transient multi-soliton states still appear, they finally give rise to nearly “turbulent” nonlinear dynamics of a “sea” of multiple DS states, which may (or may not, depending on x_m) settle on an asymptotic multi-soliton state.

On the other hand, we have also investigated the dynamics of the fundamental (single) dark soliton in Fig. 5. We have found that, in their instability region, DSs decay towards the nodeless state, as expected, if the latter is stable. However, when the nodeless state is unstable, the dynamics is as follows: after a transient stage, a breathing multiple-DS structure is formed, which may consist of 3, 4 or 5 DSs. Examples of such evolutions are shown in the insets of Fig. 5. In this case, the DS is stable in the range $2.1 < x_m < 3.1$.

The effects of varying the parameters σ and x_m , are depicted in Figs. 6 and 7, for fixed pumping spot strengths $\alpha = 2$ and $\alpha = 3$, respectively. A new dynamical feature that arises for $\alpha = 3$ and sufficiently large σ and x_m (see Fig. 7) is the emergence of a highly asymmetric “sawtooth” structure (notice that for this value of α , no stable DSs are found). Figure 8 shows how these sawtooth structures emerge from the NC when the latter is unstable. The top panel shows the the emergence of a breathing sawtooth structure from an unstable NC. Notice that the asymmetry of this configuration is produced by the amplification of the asymmetric (small) perturbation added to the NC in order to manifest its dynamical instability. We have checked that this breathing behavior persists for very long times (larger than several thou-

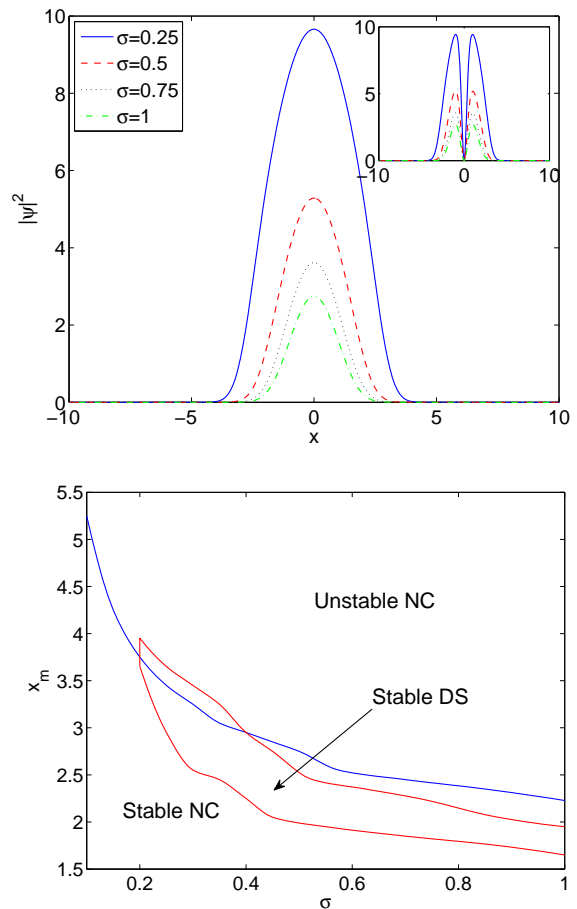


FIG. 6: (Color online) Top panel: Profiles for the nodeless clouds and dark solitons (inset) for different values of σ and fixed $\alpha = 2$ and $x_m = 2.5$. Bottom panel: Stability domain for nodeless clouds (NC) and dark solitons (DS) for $\alpha = 2$.

sands) without any apparent decay. This is due to the fact that, for these parameter values, the steady state sawtooth configuration is unstable (see the spectrum depicted in the inset of the top panel in Fig. 8) and thus the cloud cannot decay to this state. For other parameter values, the emerging sawtooth structures settle to stationary configurations without any breathing as can be seen in the bottom panel of Fig. 8. This case corresponds to parameter values inside the elongated island depicted in the bottom panel of Fig. 7 where these sawtooth configurations are *stable*.

The top panel of Fig. 7 depicts examples of stationary sawtooth structures. Similar to the saturation of the nodeless cloud size for large pumping spot size x_m , we have also observed a saturation of the size for the sawtooth structures for large x_m (results not shown here). It is extremely interesting that the polariton condensate is able to support stable *asymmetric* sawtooth-patterned states. Such solutions are not possible in atomic BECs. Furthermore, it is important to mention that, because of

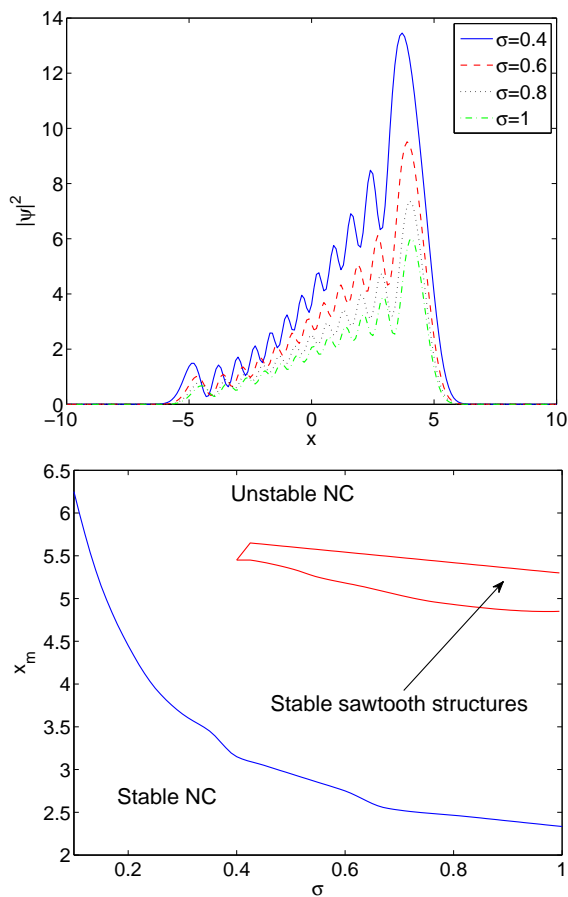


FIG. 7: (Color online) Top panel: Profiles of highly asymmetric “sawtooth” structures for different values of σ and fixed $\alpha = 3$ and $x_m = 5$. Bottom panel: Stability domain for sawtooth structures with $\alpha = 3$.

the left-to-right symmetry of our system, the sawtooth states appear in pairs (left- and right-handed sawtooth structures). In this work, for simplicity, we chose to only depict one family as the other one is symmetric with respect to the center of the cloud.

Finally, although our results already suggest that non-linear excitations in the form of dark solitons should spontaneously emerge in polariton BECs, we offer some alternative dynamical schemes for producing such excitations inspired by experimental realizations within their atomic BEC counterparts [20, 25], which also appear to be within reach for the case of polaritons; see e.g. the very recent work of Ref. [19] and references therein. One possible nucleating mechanism for dark solitons is by *dragging an obstacle*—in the form of the potential of Eq. (6)—sufficiently fast through the condensate (see Refs. [25] and [19] for relevant experimental observations in atomic and polariton condensates, respectively). Examples of this effect are shown in Fig. 9. For the relatively strong harmonic confinement considered in Eq. (1), we have found that at most two DSs can survive, due to their relatively

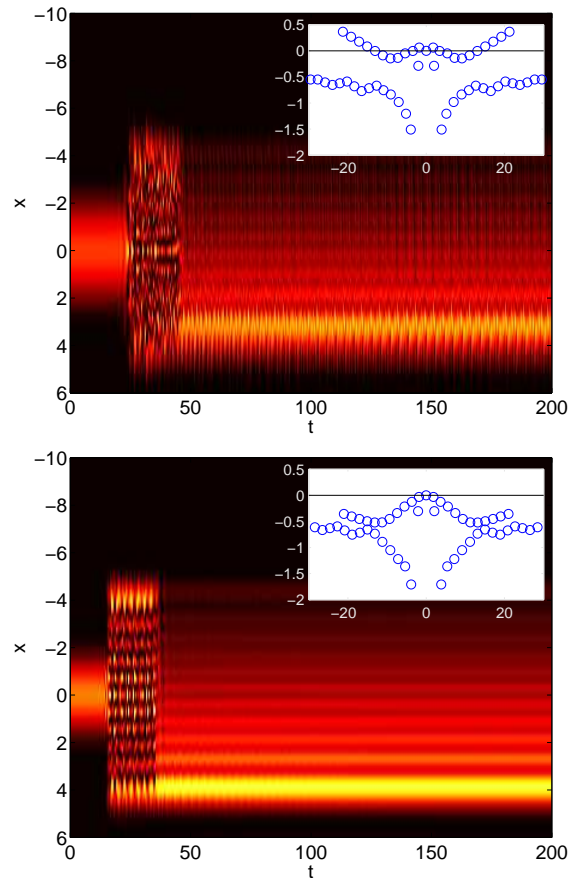


FIG. 8: (Color online) Density plots showing the evolution of unstable nodeless clouds to a breathing sawtooth structure for $\sigma = 0.5$ (top) and a non-breathing sawtooth structure for $\sigma = 1$ (bottom) with $x_m = 5$. The inset in the top panel shows the linearization spectrum of the *unstable* sawtooth steady state about which the system oscillates about for long times. The inset in the bottom panel corresponds to the linearization spectrum for the *stable* sawtooth steady state that the system asymptotes to.

large size. In this case, as shown in the top panel of Fig. 9, although three (or even four) DS can be seen being emitted out of the defect path, through collisions they eventually decay down to two, that continue to interact. The DS nature of these structures can be seen through the phase jump of π shown (together with its profile) in the inset. Chains of dark solitons (alias “dark soliton trains”) can be produced by this dragging defect mechanism if one chooses a weaker harmonic trap $\Omega^2 x^2/2$ [instead of x^2 as in Eq. (1)], with a trap strength Ω sufficiently small. In fact, as depicted in the bottom panel of Fig. 9, a weaker trapping with $\Omega = 0.04$ (corresponding to a considerably wider condensate) allows for the formation of a train of DSs that propagates initially in the opposite direction of the dragging defect. However, contrary to the Hamiltonian case of atomic BECs where the distance between the generated DSs appears to be

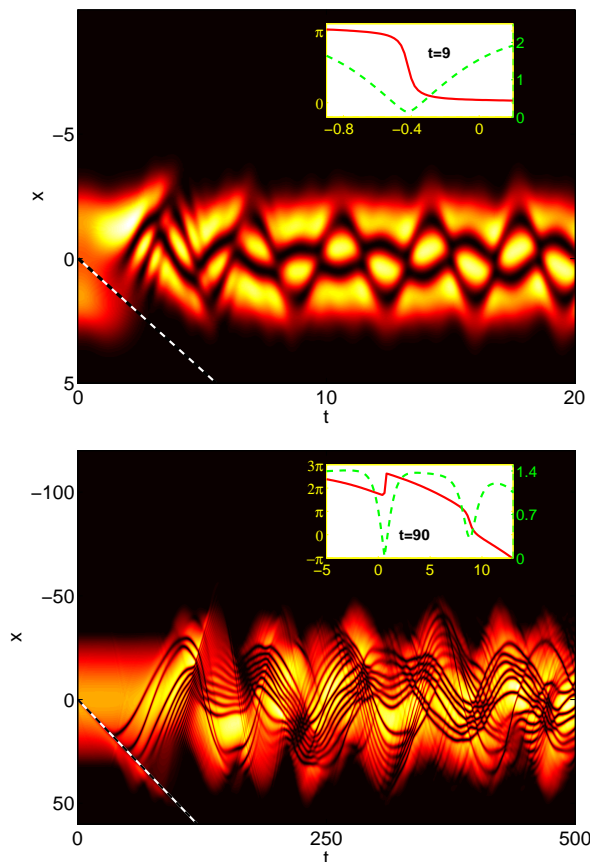


FIG. 9: (Color online) Nucleation of dark solitons by a dragging defect traversing a nodeless cloud. Depicted are the density plots of the nodeless cloud as it is traversed by the dragging defect. The dashed line represents the trajectory of the defect. The case depicted in the top panel corresponds to a tighter confinement with trap frequency $\Omega = 1$, and parameter values $\alpha = 1.0$, $\sigma = 0.35$ and $x_m = 2.8$ whereas $V_0 = 8$, $v = 0.9$ and $\epsilon^2 = 4$. The bottom panel corresponds to a weaker harmonic trapping with trap frequency $\Omega = 0.04$, and $\alpha = 0.1$, $\sigma = 0.08$ and $x_m = 44.5$, while $V_0 = 1$, $v = 0.5$ and $\epsilon^2 = 0.16$. The insets show the profile ([green] dashed line) and its corresponding phase ([red] solid line) at the indicated times.

approximately constant [28], here DSs interact strongly with each other and with the background cloud, setting it in oscillation. This might also be due to the unstable nature of the underlying NC cloud for this parameter set. Again the DS nature is visible from the π phase jump at each of the nonlinear excitations shown in the inset.

Another possible nucleation mechanism for DSs is by nonlinear interference (see, e.g., Ref. [21] for a discussion in the context of atomic BECs). This mechanism can be realized by splitting the condensate into two fragments by adiabatically inducing a potential barrier in the central portion of a stationary nodeless cloud, and subsequently releasing the fragments by suddenly removing the barrier that separates them. This “nonlinear inter-

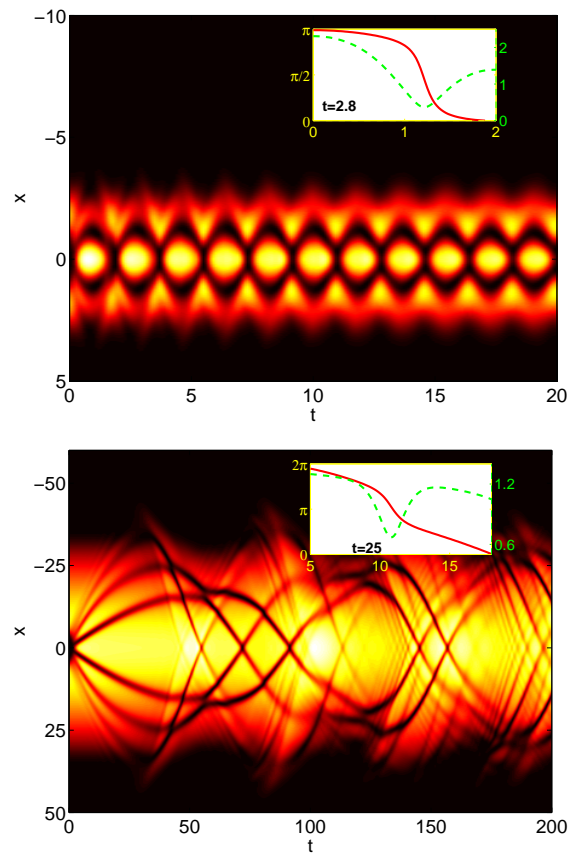


FIG. 10: Nucleation of dark soliton pairs by nonlinear interference of colliding condensate fragments. The plots depict the density of the evolution of a cloud created in a double well and allowed to interfere by removing the central barrier. Parameter values are: (top) $\alpha = 1.0$, $\sigma = 0.35$ and $x_m = 2.8$ whereas $V_0 = 17$ and $\epsilon^2 = 1$, $\Omega = 1$; (bottom) $\alpha = 0.1$, $\sigma = 0.08$ and $x_m = 44.5$ whereas $V_0 = 4$ and $\epsilon^2 = 16$, while the trap frequency is $\Omega = 0.04$. The insets show the profile ([green] dashed line) and its corresponding phase ([red] solid line) at the indicated times.

ference method” was used in atomic BEC experiments to demonstrate the generation of vortex structures [29] (see also theoretical work in Ref. [30]) and dark solitons [20, 23, 31]. Figure 10 depicts two samples of this nucleation mechanism where two polariton condensates, initially placed in a double well potential, are released in the harmonic trap and allowed to interfere. Again we show the scenarios of strong (top) and weak(er) harmonic confinement (bottom). We considered an initial situation where a barrier of the same shape as (but wider than) the obstacle considered before [cf. Eq. 6] is superposed at the center of the harmonic trap. At $t = 0$ the barrier is removed, thus allowing the two portions of the condensate to mix and interfere. As can be seen in the top panel of Fig. 10, a pair of dark pulses is formed; but contrary to the case of the soliton trains nucleated by the dragging defect, we observe that the DSs nucleated

by the nonlinear interference mechanism move relatively fast away from each other towards the edge of the condensate. Notice that, as again shown in the inset, the phase jumps of approximately π indicate that these are pairs of genuine DSs. The bottom panel shows the case of weaker confinement where in this case more than one pair of nonlinear excitations is produced by the nonlinear interference.

IV. CONCLUSIONS

In this work, we considered and studied a complex Gross-Pitaevskii model describing the quasi-one-dimensional dynamics of polariton condensates. Our motivation was to understand the fundamental differences between polariton condensates and their atomic (Hamiltonian BECs) counterparts. We found that the specific pumping and damping terms that have been argued as being relevant to polariton condensates case offer a wide range of unexpected features when compared to atomic condensates.

The fundamental nodeless state (regarded as the “ground state”) of the system was found to become unstable through a variety of mechanisms, while excited states—in the form of single- or multiple-dark solitons—were found to result from the instability of the nodeless state. The fundamental excited state, namely the single dark soliton was also found to be subject to instabilities, leading to either spontaneous formation of multi-dark soliton states or even to emergence of a “dark-soliton-turbulence” (when highly unstable). All these are dynamical manifestations which significantly distinguish the polaritonic case from the atomic BEC variant of the problem, yet we have intuitively attributed them to the emerging competition of length scales (among the intrinsic length scale of the trapped system and the length scale of the applied forcing). We also observed the emergence of *stable asymmetric* sawtooth-like configurations which are not present in atomic BECs.

Finally, other techniques, namely nucleation of dark

solitons by dragging an obstacle through the condensate and through nonlinear interference of colliding condensate fragments, have been studied. These were adapted from the atomic condensate case in order to produce fundamental nonlinear excitations—in the form of dark solitons. It was shown that both techniques were efficient in doing so.

There are numerous interesting avenues that this work opens in the way of future directions. On the one hand, it would be useful to try to develop analytical tools to understand the instability of dark solitons in polariton condensates, as well as that of the backgrounds (i.e., the nodeless clouds) on which these “live”. On the other hand, it would be interesting to extend some of the present considerations, such as the spectral analysis of stationary states, or the nonlinear interference technique for producing coherent structures in the 2D case to examine some of the theoretical and potentially even experimentally relevant (in the latter case) results thereof. Such studies are currently in progress and will be reported in future publications.

Acknowledgments

J.C. acknowledges financial support from the MICINN project FIS2008-04848. A.S.R. gratefully acknowledges the hospitality from the Department of Mathematics of the University of Massachusetts, financial support from FCT through grant SFRH/BSAB/1035/2010, and the use of computational resources from GOE-Inesc Porto. R.C.G. gratefully acknowledges the hospitality of the Grupo de Física No Lineal (GFNL, University of Sevilla, Spain) and support from NSF-DMS-0806762, Plan Propio de la Universidad de Sevilla, Grant No. IAC09-I-4669 of Junta de Andalucía and Ministerio de Ciencia e Innovación, Spain. P.G.K. acknowledges the support from NSF-DMS-0806762 and from the Alexander von Humboldt Foundation. The work of D.J.F. was partially supported by the Special Account for Research Grants of the University of Athens.

-
- [1] J. Kasprzak, M. Richard, S. Kundermann, A. Baas, P. Jeambrun, J.M.J. Keeling, F.M. Marchetti, M.H. Szymańska, R. André, J.L. Staehli, V. Savona, P.B. Littlewood, B. Deveaud, and L.S. Dang, *Nature* **443**, 409 (2006); R. Balili, V. Hartwell, D. Snoke, L. Pfeiffer, and K. West, *Science* **316**, 1007 (2007); W. Lai, N.Y. Kim, S. Utsunomiya, G. Roumpos, H. Deng, M.D. Fraser, T. Byrnes, P. Recher, N. Kumada, T. Fujisawa, and Y. Yamamoto, *Nature* **450**, 529 (2007); H. Deng, G.S. Solomon, R. Hey, K.H. Ploog, and Y. Yamamoto, *Phys. Rev. Lett.* **99**, 126403 (2007).
 - [2] C.J. Pethick and H. Smith, *Bose-Einstein condensation in dilute gases* (Cambridge University Press, Cambridge, 2002).
 - [3] L.P. Pitaevskii and S. Stringari, *Bose-Einstein Condensation* (Oxford University Press, Oxford, 2003).
 - [4] G. Björk, S. Machida, Y. Yamamoto, and K. Igeta, *Phys. Rev. A* **44**, 669 (1991); C. Weisbuch, M. Nishioka, A. Ishikawa, and Y. Arakawa, *Phys. Rev. Lett.* **69**, 3314 (1992).
 - [5] A. Amo, J. Lefrère, S. Pigeon, C. Abrados, C. Ciuti, I. Carusotto, R. Houdré, E. Giacobino and A. Bramati, *Nature Physics* **5**, 805 (2009).
 - [6] K.G. Lagoudakis, M. Wouters, M. Richard, A. Baas, I. Carusotto, R. André, L.S. Dang, B. Deveaud-Plédran, *Nature Physics* **4**, 706 (2008).
 - [7] M.D. Fraser, G. Roumpos and Y. Yamamoto, *New J. Phys.* **11**, 113048 (2009).

- [8] A. Amo, D. Sanvitto, F.P. Laussy, D. Ballarini, E. del Valle, M.D. Martin, A. Lemaître, J. Bloch, D.N. Krizhanovskii, M.S. Skolnick, C. Tejedor and L Viña, *Nature* **457**, 291 (2009).
- [9] A. Amo, T.C.H. Liew, C. Adrados, R. Houdré, E. Giacobino, A.V. Kavokin and A. Bramati, *Nature Photonics* **4**, 361 (2010).
- [10] S.I. Tsintzos, N.T. Pelekanos, G. Konstantinidis, Z. Hatzopoulos and P.G. Savvidis, *Nature* **453**, 372 (2008).
- [11] J. Keeling and N.G. Berloff, *Phys. Rev. Lett.* **100**, 250401 (2008).
- [12] M.O. Borgh, J. Keeling and N.G. Berloff, *Phys. Rev. B* **81**, 235302 (2010).
- [13] P.G. Kevrekidis, D.J. Frantzeskakis, and R. Carretero-González, *Emergent Nonlinear Phenomena in Bose-Einstein Condensates: Theory and Experiment* (Springer-Verlag, Heidelberg, 2008).
- [14] M. Wouters and I. Carusotto, *Phys. Rev. Lett.* **99**, 140402 (2007).
- [15] M. Wouters, I. Carusotto and C. Ciuti, *Phys. Rev. B* **77**, 115340 (2008).
- [16] C. Ciuti and I. Carusotto, *Phys. Stat. Sol (b)* **242**, 2224 (2005).
- [17] H. Deng, H. Haug, Y. Yamamoto, *Rev. Mod. Phys.* **82**, 1489 (2010).
- [18] R. Idrissi Kaitouni, O. El Daïf, A. Baas, M. Richard, T. Paraïso, P. Lugan, T. Guillet, F. Morier-Genoud, J.D. Ganière, J.L. Staehli, V. Savona, and B. Deveaud, *Phys. Rev. B* **74**, 155311 (2006); O. El Daïf, A. Baas, T. Guillet, J.-P. Brantut, R.I. Kaitouni, J.L. Staehli, F. Morier-Genoud, and B. Deveaud, *Appl. Phys. Lett.* **88**, 061105 (2006); D. Bajoni, E. Peter, P. Senellart, J.L. Smirr, I. Sagnes, A. Lemaître, and J. Bloch, *Appl. Phys. Lett.* **90**, 051107 (2007); D. Bajoni, P. Senellart, E. Wertz, I. Sagnes, A. Miard, A. Lemaître, and J. Bloch, *Phys. Rev. Lett.* **100**, 047401 (2008); R. Cerna, D. Sarchi, T.K. Paraïso, G. Nardin, Y. Léger, M. Richard, B. Pietka, O. El Daïf, F. Morier-Genoud, V. Savona, M. T. Portella-Oberli, and B. Deveaud-Plédran, *Phys. Rev. B* **80**, 121309(R) (2009); M. Wouters, T.C.H. Liew, and V. Savona *Phys. Rev. B* **82**, 245315 (2010).
- [19] A. Amo, S. Pigeon, D. Sanvitto, V. G. Sala, R. Hivet, I. Carusotto, F. Pisanello, G. Lemenager, R. Houdre, E. Giacobino, C. Ciuti, and A. Bramati, arXiv:1101.2530.
- [20] A. Weller, J.P. Ronzheimer, C. Gross, J. Esteve, M.K. Oberthaler, D.J. Frantzeskakis, G. Theocharis and P.G. Kevrekidis, *Phys. Rev. Lett.* **101**, 130401 (2008); G. Theocharis, A. Weller, J.P. Ronzheimer, C. Gross, M.K. Oberthaler, P.G. Kevrekidis, and D.J. Frantzeskakis, *Phys. Rev. A* **81**, 063604 (2010).
- [21] D. J. Frantzeskakis, *J. Phys. A: Math. Theor.* **43**, 213001 (2010).
- [22] C. Becker, S. Stellmer, P. Soltan-Panahi, S. Dörscher, M. Baumert, E.-M. Richter, J. Kronjäger, K. Bongs, and K. Sengstock, *Nature Physics* **4**, 496 (2008); S. Stellmer, C. Becker, P. Soltan-Panahi, E.-M. Richter, S. Dörscher, M. Baumert, J. Kronjäger, K. Bongs, and K. Sengstock, *Phys. Rev. Lett.* **101**, 120406 (2008).
- [23] I. Shomroni, E. Lahoud, S. Levy, and J. Steinhauer, *Nature Phys.* **5**, 193 (2009).
- [24] Z. Dutton, M. Budde, C. Slowe, and L. V. Hau, *Science* **293**, 663 (2001).
- [25] P. Engels and C. Atherton, *Phys. Rev. Lett.* **99**, 160405 (2007).
- [26] E. Cancellieri, F.M. Marchetti, M.H. Szymańska and C. Tejedor, *Phys. Rev. B* **82**, 224512 (2010)
- [27] M. Wouters and I. Carusotto, *Phys. Rev. Lett.* **105**, 020602 (2010).
- [28] R. Carretero-González, P.G. Kevrekidis, D.J. Frantzeskakis, B.A. Malomed, S. Nandi, and A.R. Bishop, *Math. Comput. Simul.* **74**, 361 (2007).
- [29] D.R. Scherer, C.N. Weiler, T.W. Neely, and B.P. Anderson, *Phys. Rev. Lett.* **98**, 110402 (2007).
- [30] R. Carretero-González, N. Whitaker, P.G. Kevrekidis, and D.J. Frantzeskakis. *Phys. Rev. A* **77**, 023605 (2008); R. Carretero-González, B.P. Anderson, P.G. Kevrekidis, D.J. Frantzeskakis, and C.N. Weiler, *Phys. Rev. A* **77**, 033625 (2008).
- [31] J.J. Chang, P. Engels, and M.A. Hoefer, *Phys. Rev. Lett.* **101**, 170404 (2008).